to-LDA 'over-depressurization' and a narrow pressure hysteresis in the reversible transformation of the two phases[7,8].

Taken together, our findings strongly argue for the HDA–LDA transformation being a first-order phase transformation. Structurally, HDA and LDA resemble[24–27] high-density liquid water (HDL) and low-density liquid water (LDL), respectively, and the present results thus also support the liquid–liquid critical-point theory, which holds that HDL and LDL transform into each other through a discontinuous, first-order process. Finally, we note that a clear polyamorphic phase separation has already been observed in the Al_2O_3–Y_2O_3 system[28,29], and may be seen in other network-forming amorphous materials[30,31]. □

Received 5 July; accepted 3 September 2002; doi:10.1038/nature01106.

1. Debenedetti, P. G. One substance, two liquids? *Nature* **392,** 127–129 (1998).
2. Sastry, S., Debenedetti, P. G., Sciortino, F. & Stanley, H. E. Singularity-free interpretation of the thermodynamics of supercooled water. *Phys. Rev. E* **53,** 6144–6154 (1996).
3. Rebelo, L. P. N., Debenedetti, P. G. & Sastry, S. Singularity-free interpretation of the thermodynamics of supercooled water. II. Thermal and volumetric behavior. *J. Chem. Phys.* **109,** 626–633 (1998).
4. Poole, P. H., Sciortino, F., Essmann, U. & Stanley, H. E. Phase behaviour of metastable water. *Nature* **360,** 324–328 (1992).
5. Franzese, G. & Stanley, H. E. Liquid-liquid critical point in a Hamiltonian model for water: analytic solution. *J. Phys. Condens. Matter* **14,** 2201–2209 (2002).
6. Floriano, M. A., Handa, Y. P., Klug, D. D. & Whalley, E. Nature of the transformations of ice I and low-density amorphous ice to high-density amorphous ice. *J. Chem. Phys.* **91,** 7187–7192 (1989).
7. Mishima, O., Takemura, K. & Aoki, K. Visual observations of the amorphous-amorphous transition in H_2O under pressure. *Science* **254,** 406–408 (1991).
8. Mishima, O. Reversible first-order transition between two water amorphs at ~0.2 GPa and ~135 K. *J. Chem. Phys.* **100,** 5910–5912 (1994).
9. Moynihan, C. T. *Ann. NY Acad. Sci.* **484,** 94 (1986); **484,** 287 (1986).
10. Mishima, O. Relationship between melting and amorphization of ice. *Nature* **384,** 546–549 (1996).
11. Suzuki, Y., Takasaki, Y., Tominaga, Y. & Mishima, O. Low-frequency Raman spectra of amorphous ices. *Chem. Phys. Lett.* **319,** 81–84 (2000).
12. Loerting, T. *et al.* A second distinct structural "state" of high-density amorphous ice at 77 K and 1 bar. *Phys. Chem. Chem. Phys.* **3,** 5355–5357 (2001).
13. Klug, D. D., Mishima, O. & Whalley, E. Raman spectrum of high-density amorphous ice. *Physica B* **139 & 140,** 475–478 (1986).
14. Tulk, C. A. *et al.* Structural studies of several distinct metastable forms of amorphous ice. *Science* **297,** 1320–1323 (2002).
15. Sivakumar, T. C., Schuh, D., Sceats, M. G. & Rice, S. A. The 2500–4000 cm^{-1} Raman and infrared spectra of low density amorphous solid water and of polycrystalline ice I. *Chem. Phys. Lett.* **48,** 212–218 (1977).
16. Handa, Y. P., Mishima, O. & Whalley, E. High-density amorphous ice. III. Thermal properties. *J. Chem. Phys.* **84,** 2766–2770 (1986).
17. Klug, D. D., Mishima, O. & Whalley, E. High-density amorphous ice. IV. Raman-spectrum of the uncoupled O-H and O-D oscillators. *J. Chem. Phys.* **86,** 5323–5328 (1987).
18. Gromitskaya, E. L., Stal'gorova, O. V., Brazhkin, V. V. & Lyapin, A. G. Ultrasonic study of the nonequilibrium pressure-temperature diagram of H_2O ice. *Phys. Rev. B* **64,** 094205 (2001).
19. Mishima, O. & Suzuki, Y. Vitrification of emulsified liquid water under pressure. *J. Chem. Phys.* **115,** 4199–4202 (2001).
20. Balagurov, A. M. *et al.* Neutron-diffraction study of phase-transitions of high-pressure metastable ice-VIII. *JETP Lett.* **53,** 30–34 (1991).
21. Poole, P. H. *et al.* Effect of hydrogen bonds on the thermodynamic behavior of liquid water. *Phys. Rev. Lett.* **73,** 1632–1635 (1994).
22. Truskett, T. M., Debenedetti, P. G. & Sastry, S. A single-bond approach to orientation-dependent interactions and its implications for liquid water. *J. Chem. Phys.* **111,** 2647–2656 (1999).
23. Debenedetti, P. G. *Metastable Liquids* (Princeton Univ. Press, 1996).
24. Floriano, M. A., Whalley, E., Svensson, E. C. & Sears, V. F. Structure of high-density amorphous ice by neutron diffraction. *Phys. Rev. Lett.* **57,** 3062–3064 (1986).
25. Bellissent-Funel, M.-C. & Bosio, L. A neutron scattering study of liquid D_2O under pressure and at various temperatures. *J. Chem. Phys.* **102,** 3727–3735 (1995).
26. Soper, A. K. & Ricci, M. A. Structures of high-density and low-density water. *Phys. Rev. Lett.* **84,** 2881–2884 (2000).
27. Finney, J. L. *et al.* Structures of high and low density amorphous ice by neutron diffraction. *Phys. Rev. Lett.* **88,** 225503 (2002).
28. Aasland, S. & McMillan, P. F. Density-driven liquid–liquid phase separation in the system Al_2O_3–Y_2O_3. *Nature* **369,** 633–636 (1994).
29. Wilding, M. C. & McMillan, P. F. Polyamorphic transitions in yttria-alumina liquids. *J. Non-Cryst. Solids* **293–295,** 357–365 (2001).
30. Katayama, Y. *et al.* A first-order liquid–liquid phase transition in phosphorus. *Nature* **403,** 170–173 (2000).
31. Deb, S. K., Wilding, M., Somayazulu, M. & McMillan, P. F. Pressure-induced amorphization and an amorphous–amorphous transition in densified porous silicon. *Nature* **414,** 528–530 (2001).

Acknowledgements We thank S. Sastry and P. G. Debenedetti for discussions and comments, and N. Kitamura for information on silica glass.

Competing interests statement The authors declare that they have no competing financial interests.

Correspondence and requests for information should be addressed to O.M. (e-mail: mishima.osamu@nims.go.jp).

Directly measured mid-depth circulation in the northeastern North Atlantic Ocean

A. S. Bower*, B. Le Cann†, T. Rossby‡, W. Zenk§, J. Gould‖, K. Speer¶ P. L. Richardson*, M. D. Prater‡ & H.-M. Zhang#‡

* *Woods Hole Oceanographic Institution, Woods Hole, Massachusetts 02543, USA*
† *Laboratoire de Physique des Océans, CNRS, UFR Sciences, BP809, 29285 Brest, France*
‡ *Graduate School of Oceanography, University of Rhode Island, Kingston, Rhode Island 02881, USA*
§ *Institut für Meereskunde, Christian-Albrechts-Universität, D-24105 Kiel, Germany*
‖ *Southampton Oceanography Centre, Empress Dock, Southampton SO14 3ZH, UK*
¶ *Department of Oceanography, Florida State University, Tallahassee, Florida 32306, USA*

The circulation of water masses in the northeastern North Atlantic Ocean has a strong influence on global climate owing to the northward transport of warm subtropical water to high latitudes[1]. But the ocean circulation at depths below the reach of satellite observations is difficult to measure, and only recently have comprehensive, direct observations of whole ocean basins been possible[2–4]. Here we present quantitative maps of the absolute velocities at two levels in the northeastern North Atlantic as obtained from acoustically tracked floats. We find that most of the mean flow transported northward by the Gulf Stream system at the thermocline level (about 600 m depth) remains within the subpolar region, and only relatively little enters the Rockall trough or the Nordic seas. Contrary to previous work[5,6], our data indicate that warm, saline water from the Mediterranean Sea reaches the high latitudes through a combination of narrow slope currents and mixing processes. At both depths under investigation, currents cross the Mid-Atlantic Ridge preferentially over deep gaps in the ridge, demonstrating that sea-floor topography can constrain even upper-ocean circulation patterns.

Warm, subtropical waters are transported to the northern North Atlantic Ocean, mainly by the Gulf Stream and its poleward extension, the North Atlantic Current (NAC), where they are cooled and transformed into the intermediate and deep water masses that spread throughout the global ocean[1]. The pathways and speeds of the currents in this region directly affect the magnitude of this thermohaline circulation, but our ability to accurately measure them has suffered from a lack of widespread direct velocity observations. As part of a large international effort to directly observe the circulation throughout this region using floats[2], several research groups from the USA, the UK, Germany and France recently collaborated in a major initiative to measure the absolute velocity at two levels in the northeastern North Atlantic using acoustically tracked subsurface floats[2,7–9] (Fig. 1). Here we present a quantitative view of the mid-depth circulation in this region and highlight some unexpected results.

Figure 2 shows the mean potential temperature (θ) distribution at the two float levels from historical data[10], and sets the hydrographic context for the velocity observations. At the upper level, the warm subtropical thermocline waters spread northward mainly in the northeastern North Atlantic. Two sources for this warm water have been proposed[5,6,11]: the warm, salty Mediterranean Water in the southeast ($\theta > 10\,^{\circ}C$) that enters the North Atlantic through the Strait of Gibraltar, and the water transported by the Gulf Stream and

Present address: National Climatic Data Center, NOAA, Asheville, North Carolina 28801, USA.

the NAC from the western basin ($5.5\,°C < \theta < 6.5\,°C$). Previous work has suggested that some of this warm water enters the Nordic seas (where it is transformed into the cold, dense water masses that fill the deep ocean basins), and that some flows generally anticlockwise around the subpolar region where it is transformed by wintertime cooling and either leaves southward along the western boundary or recirculates within the subpolar gyre[5,6,11,12].

At the lower level, the large-scale temperature contrast from southeast to northwest illustrates the competing influence of warmer, saline Deep Mediterranean Water ($\theta > 7\,°C$) and cooler, fresher Labrador Sea Water (LSW) ($\theta < 3.4\,°C$)[13]. LSW spreads into the eastern North Atlantic across the Mid-Atlantic Ridge at about 50° N (refs 13, 14). The influence of warmer, saltier Iceland–Scotland Overflow Water, which enters the northern Iceland basin through the Faroe Bank channel, is apparent along the continental slope south of Iceland and on both flanks of the Reykjanes ridge ($\theta > 3.8\,°C$)[15].

We used the float velocity data to construct maps of mean streamfunction (Fig. 3). Whereas historical circulation schemes for the upper level in the subpolar North Atlantic relied heavily on assumptions about the deep flow field[16,17], Fig. 3a provides directly measured, quantitative information on the mean currents during the sampling period. The NAC flows northward along the western boundary with typical mean speeds of 15–20 cm s^{-1}, to about 52° N. Here it turns sharply clockwise around the 'Northwest Corner', and heads eastward across the North Atlantic[18,19]. The streamlines fan out substantially owing to the branching of the NAC into several weaker currents[18,20–22], and the mean speed drops to about 2 cm s^{-1}, but they converge again where the NAC crosses the Mid-Atlantic Ridge, where the average speed is 3–4 cm s^{-1} (higher over the Charlie-Gibbs fracture zone (CGFZ) at 52–53° N, 5 cm s^{-1}). All the streamlines that cross the ridge between 50° N and 53° N turn northward into the Iceland basin, where the typical mean speed drops again to 2 cm s^{-1}. Some streamlines turn sharply

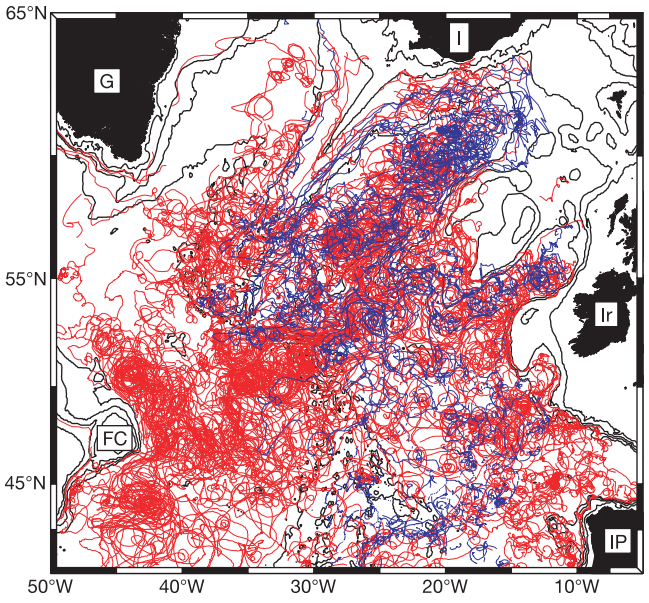

Figure 1 Float trajectories. Shown are trajectories of all 223 acoustically tracked, eddy-resolving, subsurface drifting floats launched in the northern North Atlantic in 1993–95 and 1996–2001, representing 328 float years of data. The floats were deployed at two levels: an upper-ocean thermocline density surface that ranges in depth from ~1,000 m in the subtropics to near the sea surface in the northwestern North Atlantic ($\sigma_\theta = 27.5$; red tracks; see also Fig. 2a), and an isobaric layer at 1,500–1,750 m depth, the core layer of Labrador Sea Water (LSW, blue tracks). Labelled landmarks include Greenland (G), Iceland (I), Ireland (Ir), Iberian peninsula (IP) and FC, Flemish Cap.

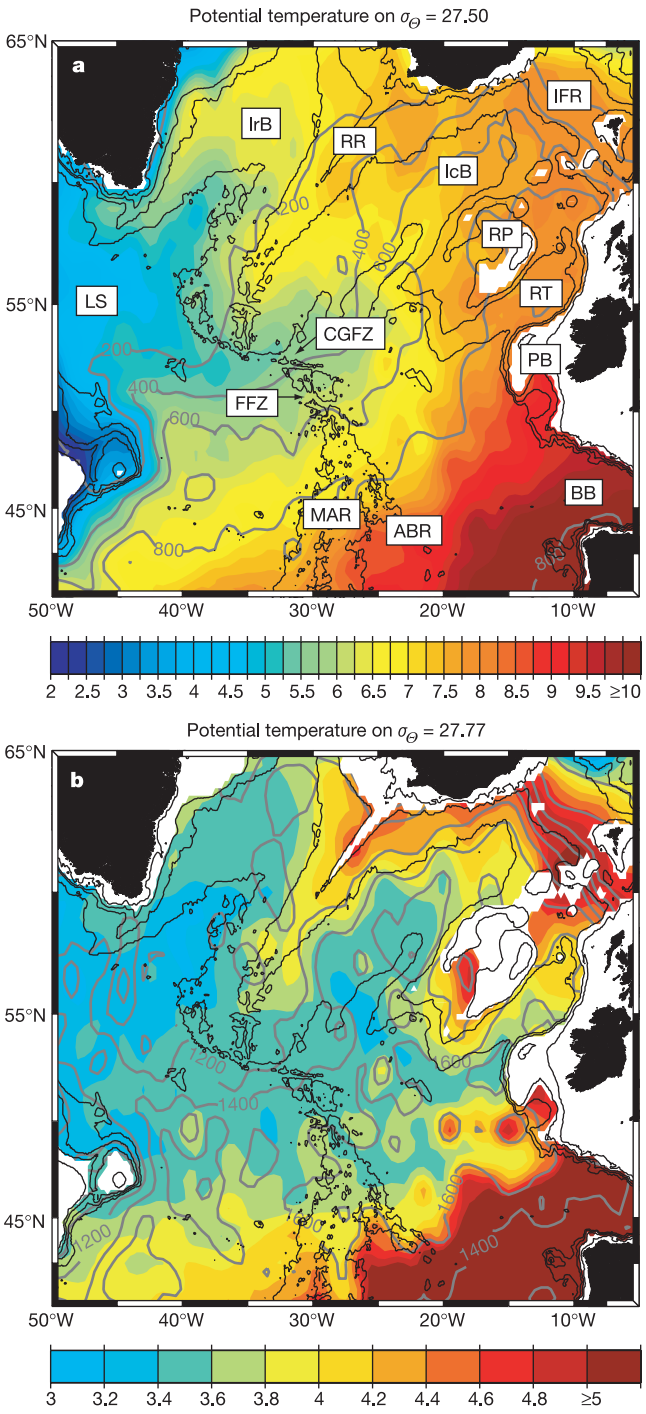

Figure 2 Mean potential temperature (colour shading) on two density surfaces in the subpolar North Atlantic corresponding to the two levels of the float data. **a**, $\sigma_\theta = 27.50$, which varies in depth (grey contours) from near the sea surface in the northwestern corner to ~1,000 m near the eastern boundary of the domain. The temperature contour interval is 0.25 °C, and bottom depth contours (m) are 200, 1,000, 2,000 and 3,000 (black contours). **b**, Same as **a** but for $\sigma_\theta = 27.77$, which ranges in depth from 1,100 m in the northwest to 1,800 m in the southeast, and with temperature contour interval of 0.20 °C. Maps are based on historical hydrographic data[10]. Temperature is shown on a density surface (rather than constant pressure surface) for the deeper float level to more accurately illustrate water mass distributions. Geographic abbreviations are: Labrador Sea (LS), Irminger basin (IrB), Reykjanes ridge (RR), Iceland basin (IcB), Iceland–Faroes ridge (IFR), Rockall plateau (RP), Rockall trough (RT), Porcupine bank (PB), Bay of Biscay (BB), Azores–Biscay rise (ABR), Mid-Atlantic Ridge (MAR), Faraday fracture zone (FFZ), Charlie-Gibbs fracture zone (CGFZ).

anticlockwise, cross back over the ridge and turn abruptly northward along the western flank of the Reykjanes ridge to form the Irminger Current, while other streamlines penetrate farther north into the Iceland basin and return southwestward along the eastern flank of the ridge before they too cross into the Irminger basin. Speeds along the eastern and western flanks of the ridge are 4–5 and 5–7 cm s^{-1}, respectively. Much weaker mean speeds are indicated in the southeastern quadrant of the study area.

As well as providing a large-scale quantitative view of the thermocline-level circulation, this map reveals a number of unexpected features. First, near the eastern boundary, the mean streamlines are mostly zonal with embedded recirculations, and there is little evidence of a continuous, broad-scale eastern boundary current advecting Mediterranean Water northward from the Iberian peninsula into the subpolar region, as has been described previously[5,6,23]. Other studies have shown that Mediterranean Water is transported northward along the eastern boundary by a narrow (~50 km) slope current (not resolved here) at least as far north as the northern Bay of Biscay[24], but Fig. 3a and individual float tracks indicate that water in this slope current is diverted into the ocean interior and recirculated, particularly at capes and other boundary protrusions. Very few of the floats launched near the eastern boundary south of 52° N drifted northward across that parallel[7]. Mediterranean Water probably penetrates north of 52° N mainly by mixing with the NAC in the complex area southwest of Porcupine bank[11]. Second, almost all of the NAC mean flow crossing the ridge turns northward into the Iceland basin, and relatively little passes through Rockall trough. (In fact none of the NAC streamlines passes through Rockall trough, but owing to statistical uncertainties in the mean velocity estimates, we cannot rule out the possibility of about 2×10^3 m^2 s^{-1} (transport per unit depth) entering the trough; see Methods). This is consistent with recent hydrographic analysis which suggests that during the low phase of the North Atlantic Oscillation in the late 1990s (characterized by weak westerly winds), the subpolar gyre contracted and the NAC flowed preferentially into the Iceland basin and not the Rockall trough[25,26].

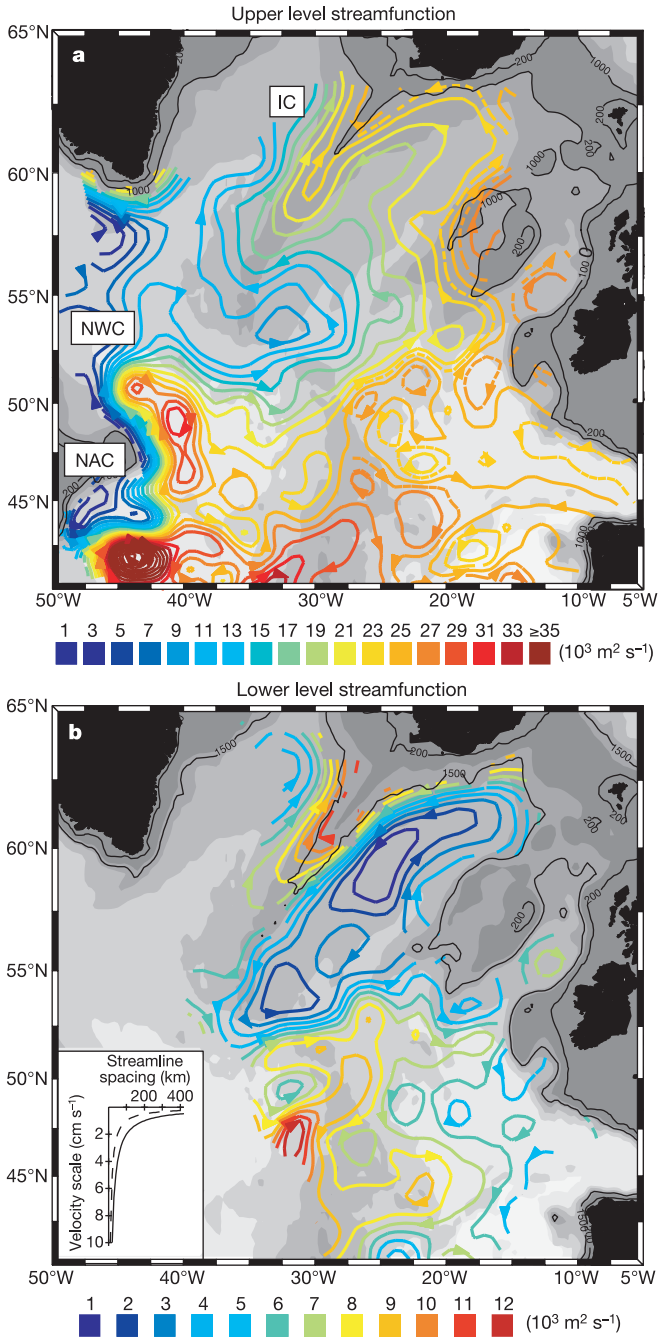

Figure 3 Mean streamfunction for the subpolar North Atlantic from subsurface float data at two levels. **a**, Upper level, thermocline, density $\sigma_\theta = 27.5$; **b**, lower level, Labrador Sea Water, depth 1,500–1,750 m. See Methods for data and mapping details. Arrowheads show the direction of flow along the contours. The inset in **b** gives speed in cm s^{-1} as a function of line separation (solid line for **a**, dashed for **b**). The colour bars below **a** and **b** give volume transport for a one-metre-thick layer. Note that two higher-resolution contours (dashed), 24,000 and 26,000 m^2 s^{-1}, have been added near the eastern boundary. Labelled features are: North Atlantic Current (NAC), 'Northwest Corner' (NWC) and Irminger Current (IC).

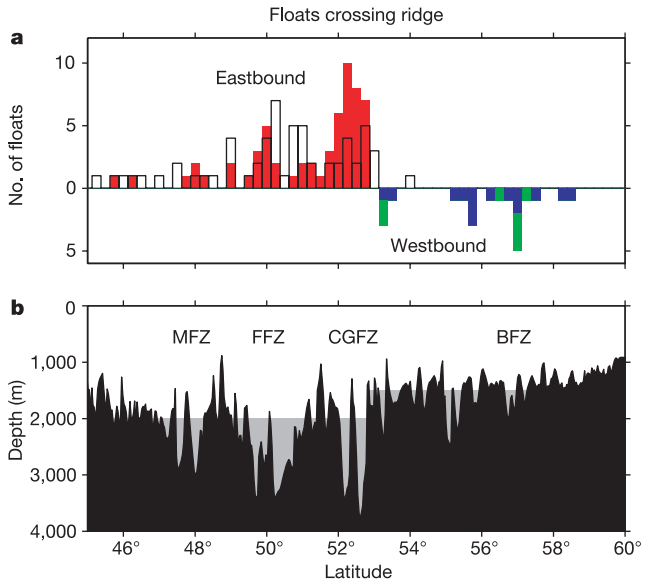

Figure 4 Floats crossing the Mid-Atlantic Ridge. **a**, Distribution of latitudes where floats crossed the Mid-Atlantic Ridge. **b**, Depth of ridge crest as a function of latitude. Floats in the North Atlantic Current at the upper level crossed the ridge eastbound preferentially over the Charlie-Gibbs fracture zone (CGFZ; 31/61), the Faraday fracture zone (FFZ; 11/61), and to a lesser extent, the Maxwell fracture zone (MFZ; 4/61) (red bars; float depths 200–800 m). The distribution of float deployment latitudes, unfilled bars, is significantly different from the distribution of crossing latitudes, suggesting that the floats were funnelled over the various fracture zones. Floats crossed the Reykjanes ridge from east to west north of 53° N at both levels (blue for upper level, green for lower level) mainly through the Bight fracture zone (BFZ) and two unnamed gaps near 53.5° N and 55° N. North of 53° N, the gaps are not aligned east–west and the distribution of float crossing latitudes is therefore somewhat wider around these gaps.

The third unexpected feature is that none of the streamlines, and none of the floats, from the subtropics crosses over the Iceland–Faroes ridge into the Norwegian Sea, even though the $\sigma_\theta = 27.5$ potential density surface is continuous over the ridge (again we cannot preclude some flow over the ridge at this level owing to uncertainties in the mean estimates, but it is probably less than 20% of the NAC flow). This indicates that most of the warm inflow into the Norwegian Sea occurs above the level of these floats[11]. Most of the flow that enters the Iceland basin from the south must therefore exit into the Irminger basin over the Reykjanes ridge; we find that eight streamlines, or $14 \times 10^3\ m^2\ s^{-1}$, cross the ridge first eastward then westward (Fig. 3a). Fourth, we find that the eastward and westward cross-ridge currents flow preferentially over fracture zones (gaps) in the ridge, even at depths up to 1,500 m above the ridge crest. This can be seen in Fig. 3a, but is much clearer in Fig. 4, which shows a histogram of the latitude where upper-level floats crossed the ridge crest (upper panel) relative to the depth of the ridge crest (lower panel). About two-thirds of the eastbound floats (42/61) were 'funnelled' over the CGFZ and Faraday fracture zone, and a few over the Maxwell fracture zone. Although it is generally accepted that the northern branch of the NAC is topographically locked to the CGFZ, the southern branches were thought to vary considerably in their crossing latitude[20–22]. Although fewer upper-level floats crossed the ridge westbound (14), they also preferentially passed over the ridge crest near the deeper gaps, including the Bight fracture zone at 57° N. This could have important implications for the response of the NAC branches to climate-related changes in atmospheric forcing: the shape of the ridge may constrain the current branches to cross within a narrow latitudinal band even for a wide range in forcing, which in turn could affect the circulation and sea surface temperature distribution throughout the subpolar region.

The mean streamfunction map for the lower level (Fig. 3b) illustrates the 'funnelling' of LSW from west to east over the CGFZ, with speed 3–4 $cm\ s^{-1}$, some of which appears to be recirculating from the northeast. The eastward current splits into two branches at the Rockall plateau, forming a broad, weak southward flow (typical speed $\sim 0.5\ cm\ s^{-1}$) and a somewhat faster northward flow into the Iceland basin ($\sim 2\ cm\ s^{-1}$). Higher transport is indicated in the southern branch, consistent with previous hydrographic results[13]. The fastest mean currents at this level, which were found at the northern end of the Iceland basin and along the eastern flank of the Reykjanes ridge, reflect the influence of the Iceland–Scotland overflow. Mean speeds range from 6 to 10 $cm\ s^{-1}$ along this current. Half of these streamlines cross westward over the Reykjanes ridge and turn northward with speed about 4 $cm\ s^{-1}$, while the other half turn eastward at the latitude of the CGFZ. This mean streamfunction map complements a similar map of directly measured LSW circulation at 700 m west of 25° W (ref. 3), and agrees well where they overlap.

Several unanticipated circulation features also emerge from the lower-level map. Two closed, anticlockwise recirculation cells exist adjacent to the boundary current in the western Iceland basin. Although larger in spatial scale, these cells resemble similar recirculations recently observed in the Labrador and Irminger seas[3]. The individual float trajectories reveal that Iceland–Scotland Overflow Water flows westward into the Irminger Sea not only through the northern part of the CGFZ[15,27], but also through deeper gaps in the highly fractured southern one-third of the Reykjanes ridge. Five of the seven deep floats that crossed the ridge westbound did so near the Bight fracture zone at 57° N, while the two others passed westward through a gap just north of the CGFZ.

Similarities in the flow pattern at the two levels include eastward flow over the CGFZ and the clockwise circulation around the Reykjanes ridge. Differences include the vertical structure on opposite sides of the ridge: on the eastern flank, the southwestward flow is significantly faster at the deeper level, while on the western flank the northeastward flow is faster at the upper level (although the vertical shear is of the same sign on both sides). Also, the closed recirculation in the northwestern Iceland basin at the lower level is absent at the upper level.

The similarity of the streamfunction patterns in Fig. 3 to the details of the sea-floor topography is notable. For example, at the upper level, the NAC closely tracks the 4,000-m isobath in the western basin. At the lower level, the southward flow in the eastern basin is clearly steered clockwise around the Azores–Biscay rise, near 45° N, 20° W (ref. 8). This is expected on the basis of the conservation of potential vorticity, f/H, where f is the Coriolis parameter and H is the fluid layer thickness. Under this conservation constraint, the Mid-Atlantic Ridge represents a significant barrier to inter-basin exchange, and the results shown here suggest that the currents flow preferentially over deeper gaps to cross the ridge. Such topographic steering may limit the ocean's response to climate variations, locking cross-ridge transports of heat and fresh water to a certain latitude band. We believe that the present data set will provide a standard for numerical simulations of the North Atlantic circulation, and a reference point for future studies of climate variability. □

Methods

Floats

The float data used in this study were collected as part of the US Atlantic Climate Change Experiment (ACCE—a component of the World Ocean Circulation Experiment), the European EUROFLOAT Project, the German Sonderforschungsbereich (SFB) Subpolar Program and the French Actions de Recherche sur la Circulation dans l'Atlantique Nord-Est (ARCANE) during the years 1996–2001. Forty additional floats from the US North Atlantic Current Study (NACS) in 1993–95 were also included[19]. The floats were tracked acoustically using an array of 18 moored sound sources that was maintained throughout the North Atlantic by the cooperating groups. Each float recorded at least one position fix and one temperature/pressure observation per day, providing high-resolution trajectories and *in situ* properties.

Float data set

The data set includes both RAFOS floats, which store all their data internally until the end of their missions, and MARVOR floats, which surface every three months to telemeter their stored data and then resubmerge to their operating depths. The upper level data set consists of (1) 116 RAFOS float tracks between 18 and 24 months in duration from the ACCE, (2) 21 MARVOR float tracks up to 60 months long from ARCANE, and (3) 40 RAFOS floats, mostly 10 months in length, from NACS, providing a total of 243 float years of data. The ACCE and NACS floats were made isopycnal by matching their compressibility to that of sea water, and making their coefficient of thermal expansion an order of magnitude less than that of sea water[28]. These floats were ballasted for the $\sigma_\theta = 27.5$ density surface (neutral surface $\gamma_n \approx 27.6$), which ranges in depth from near the sea surface in the Irminger and Labrador seas, to about 1,000 m adjacent to the European continent (Fig. 2a). Combining these isopycnal floats with the isobaric ARCANE floats, which were ballasted for 1,000 m, is justified because the latter were mainly confined to the southeastern part of the study region, where the 27.5 density surface is nearly 1,000 m deep. The deep floats comprise 25 SFB RAFOS floats at 1,500 m and 21 EUROFLOAT MARVOR floats at 1,750 m for a total of 85 float years. Combining the 1,500- and 1,750-m floats into one layer is justified on the basis of the relative lack of vertical shear between these depths.

Data analysis

The mean velocity at the two levels was estimated by grouping all the float velocity observations according to location into bins 110 km square in flat areas, and somewhat skewed along the isobaths over the continental slope and the Mid-Atlantic Ridge because the mean flows are often aligned along the topography[4]. The data density (N) exceeds 100 float days per bin in much of the North Atlantic in the upper layer, and in the eastern North Atlantic in the lower layer. The resulting mean velocity vectors were mapped into a scalar streamfunction field using standard objective analysis (OA) techniques[29]. By definition the streamfunction fields produced by the OA are non-divergent: the divergent part is of the order of Ro smaller and thus within the noise (Ro is the Rossby number, U/fL, where U and L are typical values for horizontal velocity and length scale). The covariance function has the form $f(r) = [1 + (r/r_o)]\exp(-r/r_o)$, where r is radial distance and r_o is chosen to be 100 km. To help ensure the robustness of the mean streamfunction fields, only areas where the data density exceeds 10 float days per bin were mapped.

Uncertainties

To approximate the uncertainty in the transport per unit depth entering Rockall trough and crossing over the Iceland–Faroes ridge, we first estimate the standard error in the mean velocity. Using $N = 100$ d with an average lagrangian integral timescale (T_I) of five days[8,30] and a standard deviation (s.d.) around the mean velocity of $\sim 7\ cm\ s^{-1}$ (typical for

the regions south of Rockall trough and the Iceland–Faroes ridge), in s.d./$(N/T_1)^{1/2}$, the standard error is ~1.5 cm s^{-1}. This translates to an uncertainty in transport per unit depth across the mouth of Rockall trough (two bins) and the Iceland–Faroes ridge (four bins) of $\sqrt{[2,4]} \times (110 \times 10^3\ \mathrm{m}) \times (0.015\ \mathrm{m\,s^{-1}}) \approx [2,3] \times 10^3\ \mathrm{m^2\,s^{-1}}$, where the numbers in brackets refer to the Rockall trough and the Iceland–Faroes ridge, respectively. This would be equivalent to 2.0–2.5 streamlines entering Rockall trough or crossing the Iceland–Faroes ridge, respectively.

Received 10 June; accepted 19 August 2002; doi:10.1038/nature01078.

1. Siedler, G., Church, J. & Gould, J. (eds) *Ocean Circulation and Climate—Observing and Modelling the Global Ocean* International Geophysics Series 77 (Academic, San Diego, 2001).
2. Davis, R. E. & Zenk, W. in *Ocean Circulation and Climate—Observing and Modelling the Global Ocean* International Geophysics Series 77 (eds Siedler, G., Church, J. & Gould, J.) 123–139 (Academic, San Diego, 2001).
3. Lavender, K. L., Davis, R. E. & Owens, W. B. Direct velocity measurements describe a new circulation regime in the Labrador and Irminger Seas. *Nature* **407,** 66–69 (2000).
4. Davis, R. Preliminary results from directly measuring mid-depth circulation in the tropical and South Pacific. *J. Geophys. Res.* **103,** 24619–24639 (1998).
5. Reid, J. L. On the mid-depth circulation and salinity field in the North Atlantic Ocean. *J. Geophys. Res.* **83,** 5063–5067 (1978).
6. Reid, J. L. On the contribution of Mediterranean Sea outflow to the Norwegian-Greenland Sea. *Deep-Sea Res.* **26,** 1199–1223 (1979).
7. Bower, A. S. *et al.* Warm-water pathways in the Subpolar North Atlantic: An overview of the ACCE RAFOS float programme. *WOCE Int. Newsl.* **38,** 14–16 (2000).
8. Speer, K., Gould, J. & LaCasce, J. Year-long float trajectories in the Labrador Sea Water of the eastern North Atlantic Ocean. *Deep-Sea Res. II* **46,** 165–179 (1999).
9. Le Cann, B., Speer, K. A., Serpette, A., Paillet, J. & Reynaud, T. Lagrangian observations in the intergyre North-East Atlantic during the ARCANE and EUROFLOAT projects: Early results. *WOCE Int. Newsl.* **34,** 25–27 (1999).
10. Curry, R. G. *A Database of Hydrographic Stations and Tools for Climatological Analysis* Technical Report WHOI-96-01 (Woods Hole Oceanographic Institution, Woods Hole, Massachusetts, 1996).
11. McCartney, M. S. & Mauritzen, C. On the origin of the warm inflow to the Nordic Seas. *Prog. Oceanogr.* **51,** 125–214 (2001).
12. McCartney, M. S. & Talley, L. D. Warm-to-cold conversion in the northern North Atlantic Ocean. *J. Phys. Oceanogr.* **14,** 922–935 (1984).
13. Paillet, J., Arhan, M. & McCartney, M. S. Spreading of Labrador Sea water in the eastern North Atlantic. *J. Geophys. Res.* **103,** 10223–10239 (1998).
14. Talley, L. D. & McCartney, M. S. Distribution and circulation of Labrador Sea water. *J. Phys. Oceanogr.* **12,** 1189–1205 (1982).
15. Dickson, R. R. & Brown, J. The production of North Atlantic deep water: Sources, rates, and pathways. *J. Geophys. Res.* **99,** 12319–12341 (1994).
16. Worthington, L. V. On the North Atlantic circulation. *Johns Hopkins Oceanogr. Stud.* **6,** 1–110 (1976).
17. Pollard, R., Read, J. & Holliday, P. Circulation and mode waters of the North Atlantic subpolar gyre in 1996. *WOCE Int. Newsl.* **37,** 21–27 (1999).
18. Krauss, W. The North Atlantic Current. *J. Geophys. Res.* **91,** 5061–5074 (1986).
19. Rossby, T. The North Atlantic current and surrounding waters: At the crossroads. *Rev. Geophys.* **34,** 463–481 (1996).
20. Belkin, I. M. & Levitus, S. Temporal variability of the Subarctic Front near the Charlie-Gibbs Fracture Zone. *J. Geophys. Res.* **101,** 28317–28324 (1996).
21. Sy, A., Schauer, U. & Meincke, J. The North Atlantic Current and its associated hydrographic structure above and eastwards of the Mid-Atlantic Ridge. *Deep-Sea Res.* **39,** 825–853 (1992).
22. Heywood, K. J., McDonagh, E. L. & White, M. A. Eddy kinetic energy of the North Atlantic subpolar gyre from satellite altimetry. *J. Geophys Res.* **99,** 22525–22539 (1994).
23. Iorga, M. C. & Lozier, M. S. Signatures of the Mediterranean outflow from a North Atlantic climatology, diagnostic velocity fields. *J. Geophys. Res.* **104,** 26011–26029 (1999).
24. Pingree, R. D. & LeCann, B. Structure, strength and seasonality of the slope currents in the Bay of Biscay region. *J. Mar. Biol. Assoc. UK* **70,** 857–885 (1990).
25. Bersch, M., Meincke, J. & Sy, A. Interannual thermocline changes in the northern North Atlantic. *Deep Sea Res. II* **46,** 55–75 (1999).
26. Bersch, M. NAO-induced changes of the upper-layer circulation in the northern North Atlantic Ocean. *J. Geophys. Res.* (in the press).
27. Schmitz, W. J. Jr & McCartney, M. S. On the North Atlantic circulation. *Rev. Geophys.* **31,** 29–49 (1993).
28. Rossby, H. T., Levine, E. & Conners, D. N. The isopycnal Swallow Float: A simple device for tracking water parcels in the ocean. *Prog. Oceanogr.* **14,** 511–525 (1985).
29. Freeland, H. J. & Gould, W. J. Objective analysis of meso-scale ocean circulation features. *Deep-Sea Res.* **23,** 915–923 (1976).
30. Zhang, H. M., Prater, M. D. & Rossby, T. Isopycnal Lagrangian statistics from the North Atlantic current RAFOS float observations. *J. Geophys. Res.* **106,** 13817–13836 (2001).

Acknowledgements We thank all the technicians and research assistants who contributed to this project for their help and support. We also thank H. Hunt Furey for help in the preparation of the figures. This work was supported by the US National Science Foundation, the Deutsche Forschungsgemeinschaft, the Institut Français de Recherche pour l'Exploitation de la Mer, the Centre National de la Recherche Scientifique, and the European Commission EUROFLOAT project.

Competing interests statement The authors declare that they have no competing financial interests.

Correspondence and requests for materials should be addressed to A.B. (e-mail: abower@whoi.edu).

A correlation between mid-ocean-ridge basalt chemistry and distance to continents

Eric Humler* & Jean Besse†

** Laboratoire des Geosciences Marines; and † Laboratoire de Géomagnetisme et de Palaeomagnétisme, IPGP-Université Denis Diderot, 4, Place Jussieu, 75252 Paris Cedex 05, France*

To fully understand the structure and dynamics of the Earth's convecting mantle, the origins of temperature variations within the mantle need to be resolved. Different hypotheses have been proposed to account for these temperature variations: for example, heat coming from the decay of radioactive elements or heat flowing out of the Earth's core. In addition, theoretical studies[1–5] suggest that the thermal properties of continental masses can affect mantle convection, but quantitative data that could allow us to test these models are scarce. To address this latter problem, we have examined the chemistry of mid-ocean-ridge basalt—which reflects the temperature of the source mantle[6,7]—as a function of the distance of the ridge from the closest continental margin. No correlation is observed for oceanic ridges close to subduction zones or hotspots; subduction zones probably inhibit thermal transfer between the mantle beneath continents and ocean, whereas hotspots influence the major-element chemistry of ridge basalts, which makes their interpretation with respect to mantle temperature more difficult. However, we do observe a significant correlation for mid-oceanic basalts from the Atlantic and Indian oceans. From this, we conclude that the location of continental masses relative to active ridges influences the large-scale thermal structure of the mantle and we estimate that the mantle cools by 0.05 to 0.1 °C per kilometre from the continental margins.

Major-element data for oceanic basalts are important because they can be quantitatively linked to mantle temperatures, axial depth of oceanic ridges, crustal thickness and seismic tomography[6–9]. Quantification of potential mantle temperatures based on basalt chemistry, experimental petrology and theories of melt extraction are now available[6–7,10–12]. In particular, $Na_{8.0}$ (Na_2O content corrected to 8% MgO) can be used as a proxy for the extent of melting, whereas $Fe_{8.0}$ is a proxy for the mean pressure of melting. Using the Langmuir *et al.*[7] formulation for mantle melting, basalts from shallow ridges (Kolbeinsey) with low $Na_{8.0}$ and high $Fe_{8.0}$ correspond to a solidus mantle temperature of about 1,460 °C. Deep ridges, such as the South West Indian Ridge (SWIR) with high $Na_{8.0}$ and low $Fe_{8.0}$ correspond to a solidus mantle temperature of about 1,210 °C.

The chemical composition of ancient crust can be used to determine palaeobathymetry of ancient ridge axes[13]. This approach has recently been applied to oceanic crust older than 80 Myr. The results were previously interpreted to infer that mantle temperatures during the Mesozoic were 50 °C hotter than today[14]. Such a large temperature decrease in such a short time interval cannot be reconciled with models of normal cooling of the Earth.

In the Earth, the thermal conditions at the upper boundary of the convecting mantle are not uniform. This is demonstrated in the most direct manner by the distribution of heat flow at the surface. Continental plates can act as insulating lids[1–5,15,16] thereby imposing large-scale heterogeneities at the Earth's surface. These heterogeneities could play an important role in determining the Earth's overall thermal structure. Theoretical studies[1–5] indicate that the amplitude of the process depends on the area, thickness and width of the continents, and on the duration of time during which they remain above a given area of the mantle before break-up. If continents do influence mantle temperatures, a correlation should exist between